Electronic Supplemental Information for

Cadmium hydroxide: a missing non-noble metal hydroxide electrocatalyst for the oxygen evolution reaction

Xiang Chen,*[†‡§] Haonan Wang,[†‡] Ruru Meng,[†‡] Bin Xia,[†‡] Zuju Ma*[†‡§]

[†]Key Laboratory of Metallurgical Emission Reduction & Resources Recycling (Anhui University of Technology), Ministry of Education, Maanshan 243002, P. R. China

[‡]School of Materials Science and Engineering, Anhui University of Technology, Maanshan 243002, P. R. China

[§]Key Laboratory of Green Fabrication and Surface Technology of Advanced Metal Materials (Anhui University of Technology), Ministry of Education, Maanshan 243002, P. R. China

Email: *chxiang@mail.ustc.edu.cn

*zjma@outlook.com

Contents

S1. Experimental section.

S2. Side views of the optimized geometries of relevant species during OER on $Cd(OH)_2$ (001) surface.

S3. Side views of the optimized geometries of relevant species during OER on $Co(OH)_2$ (001) surface.

S4. SEM images and TEM images $Cd(OH)_2$ prepared by using $CdCl_2$ and $CdSO_4$ as the precursors.

S5. XRD patterns of $Cd(OH)_2$ prepared by using $CdCl_2$ and $CdSO_4$ as the precursors.

S6. XPS spectra of the prepared $Cd(OH)_2$ catalysts.

S7. The OER electrocatalytic activities of $Cd(OH)_2$ prepared by using $CdCl_2$ and $CdSO_4$ as the precursors.

S8. N_2 adsorption–desorption isotherms of the $Cd(OH)_2$ catalysts.

S9. XRD pattern of $Cd(OH)_2$ catalyst after galvanostatic stability test.

S10. SEM and TEM images of $Cd(OH)_2$ catalyst after galvanostatic stability test.

S11. SEM image of $Co(OH)_2$.

S12. The OER electrocatalytic activities of $Fe(OH)_3$ and $Ni(OH)_2$.

S13. CV curves of $Cd(OH)_2$ and $Co(OH)_2$ at different scan rates.

S1. Experimental Section

Materials

$Cd(NO_3)_2·4H_2O$, $Co(NO_3)_2·6H_2O$, $Fe(NO_3)_3·9H_2O$, $Ni(NO_3)_2·6H_2O$, KOH, NaOH, HCl (≈37 wt%) and Ni foam were purchased from China National Pharmaceutical Industry Corporation Ltd. RuO_2 (99.9%) was purchased from Aladdin. Except the Ni foam was washed with diluted hydrochloric acid, water and ethanol successively, other materials were used as received without further treatment.

Synthesis of metal hydroxides

The metal hydroxides $Cd(OH)_2$, $Co(OH)_2$, $Fe(OH)_3$ and $Ni(OH)_2$ were prepared by drop by drop adding aqueous solution of sodium hydroxide to an aqueous solution of metal nitrates $Cd(NO_3)_2$, $Co(NO_3)_2$, $Fe(NO_3)_3$ and $Ni(NO_3)_2$ under mild stirring, respectively. The products were washed several times with deionized water and dried in oven at 60 ^oC for 12 h, and the metal hydroxides were obtained finally. The $Cd(OH)_2$ using other cadmium salts ($CdCl_2$ and $CdSO_4$) as the precursor also were prepared by using the same method as $Cd(NO_3)_2$ as the precursor.

Measurements and Characterization.

X-ray powder diffraction patterns were characterized on an X-ray diffractometer with Cu Kα radiation (40 kV, 30 mA, λ= 0.154 nm) at a scan rate of 5° min^{-1}. The morphology characterizations of the samples were performed using a field-emission scanning electron microscope (SEM) (JEOL JSM6335) operating at 20 kV. Transmission electron microscopy (TEM) and element mapping measurements were carried out using a JEOL JEM 2100 system operating at 200 kV. X-ray photoelectron spectroscopy (XPS) was carried out using an ESCALAB 250 X-ray photoelectron spectrometer (Thermo-VV Scientific) with Al Kα X-ray radiation. Brunauer–Emmett–Teller (BET) surface area analysis were carried out on ASAP 2460 instrument (Micromeritics, USA).

Electrochemical Measurements

The electrochemical OER measurements were carried out at room temperature in a three-electrode glass cell connected to an electrochemical workstation (CHI 660e, CH, Shanghai.). 10 mg $Cd(OH)_2$, $Co(OH)_2$ $Fe(OH)_3$, $Ni(OH)_2$ or RuO_2 catalyst and 60 μL 5 wt% Nafion were added into 2 mL isopropanol and ultrasounded for 1 h. Then 10 μL above solution was droped in Ni foam, which was used as the work electrode (geometric area is 0.25 cm^2). A platinum electrode and a saturated Ag/AgCl were used as counter and reference electrode, respectively. Freshly prepared 1 M KOH aqueous solution (PH=13.9) was used as the electrolyte. Polarization curves were obtained using linear sweep voltammetry (LSV) with a scan rate of 2 mV/s. All polarization curves were corrected for the iR compensation. The electrochemical impedance spectroscopy (EIS) was obtained in 1 M KOH solution by applying an AC voltage of 5 mV amplitude at an applied voltage 1.5 V vs. RHE in the frequency range of 0.01 Hz–100 kHz.

Calculation methods

Our calculations on the pristine $Co(OH)_2$ and $Cd(OH)_2$ (001) surface were performed using the plane-wave basis Vienna Ab-initio Simulation Package (VASP) code[S1-S3]. The projected augmented wave (PAW)[S4] potentials with the valence states *1s* for H, *2s* and *2p* for O, *3d* and *4s* for Co, and *4d* and *5s* for Cd were

used to treat the core-valence interaction. The PBE functional[S5] was chosen for the structural optimization in this work. The vacuum region was kept at 15 Å, which was thick enough to avoid artificial interaction. A Γ-centered 9×9×1 Monkhorst-Pack k-point grid and a cutoff energy of 450 eV were found to get convergent total and adsorption energies. The geometries were fully relaxed until the maximal residual force was less than 0.02 eV/Å. The $Co(OH)_2$ and $Cd(OH)_2$ (001) surfaces were modeled using a slab with a 2×2 cell in the surface direction and two atomic layers in the normal direction**1**. The bottom layer was fixed at the bulk position in the optimization of slab models.

We modeled the OER using the method developed by Norskov and coworkers,[S6, S7] who have studied the water oxidation on different metal oxide surfaces, such as TiO_2, RuO_2, and IrO_2. Free energy change $\Delta G_0 = \Delta E + \Delta ZPE - T\Delta S$, with ΔE denoting the total self-consistent energy change (reaction energy) derived from DFT calculations, ΔZPE indicating the differences in zero-point energies, and ΔS indicating the change of entropy. ZPE for the OER intermediates were obtained from the vibrational frequencies. For free gas-phase molecules, we obtained ZPE and S from thermodynamics database.[S6] The free energy of $H^+ + e^-$ has been replaced by one-half of the chemical potential of the hydrogen molecule. Under the influence of a potential bias U and an infinite pH, the free energy difference was shifted by $\Delta G\ (U, pH) = \Delta G_U + \Delta G_{pH} = -eU - kT\ln10\times pH$.

S2. Side views of the optimized geometries of relevant species during OER on $Cd(OH)_2$ (001) surface.

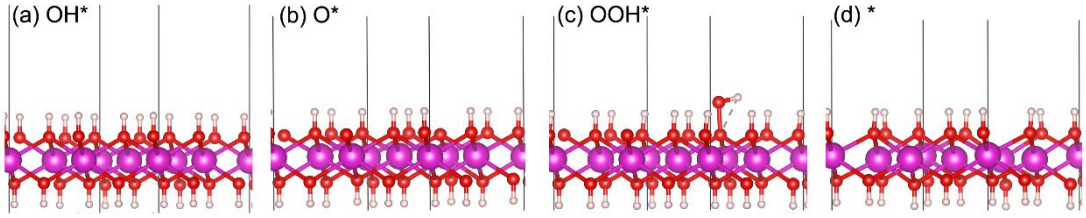

Figure S1. Side views of the optimized geometries of relevant species (OH*, O*, OOH* and *) during OER on $Cd(OH)_2$ (001) surface.

S3. Side views of the optimized geometries of relevant species during OER on $Co(OH)_2$ (001) surface.

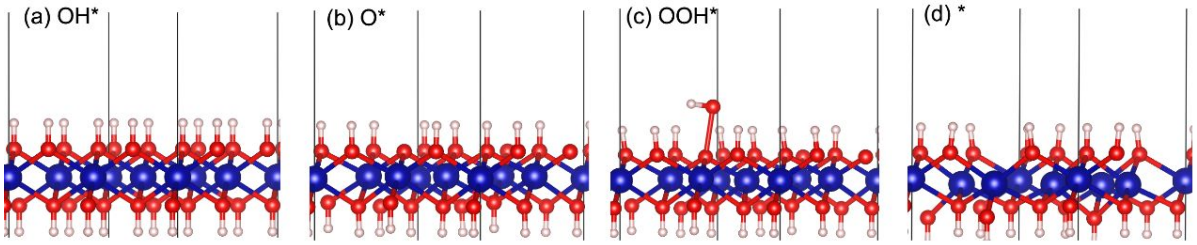

Figure S2. Side views of the optimized geometries of relevant species (OH*, O*, OOH* and *) during OER on $Co(OH)_2$ (001) surface.

S4. SEM images and TEM images $Cd(OH)_2$ prepared by using $CdCl_2$ and $CdSO_4$ as the precursors.

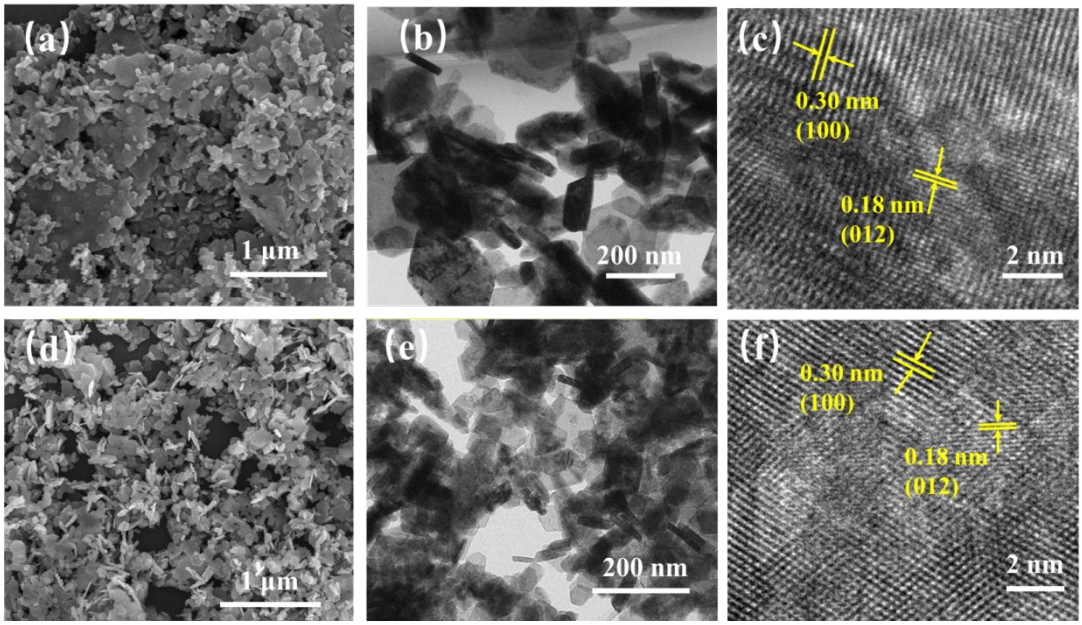

Figure S3. (a,d) SEM images, (b,e) TEM images and (c,f) HRTEM images of $Cd(OH)_2$ prepared by using $CdCl_2$ and $CdSO_4$ as the precursors, respectively.

S5. XRD patterns of $Cd(OH)_2$ prepared by using $CdCl_2$ and $CdSO_4$ as the precursors.

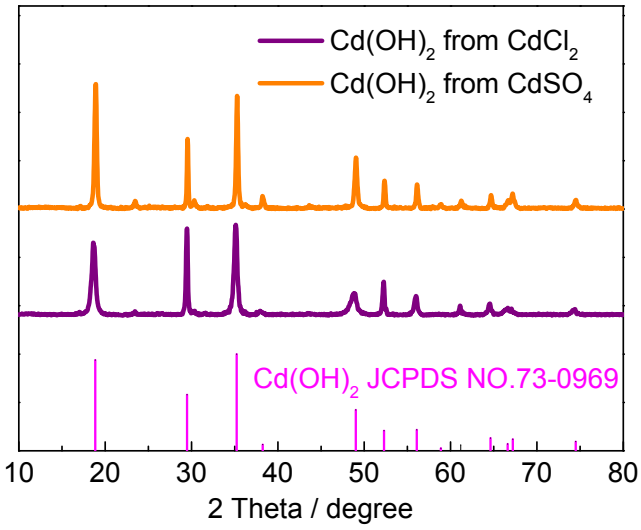

Figure S4. XRD patterns of $Cd(OH)_2$ prepared by using $CdCl_2$ and $CdSO_4$ as the precursors.

S6. XPS spectra of the prepared $Cd(OH)_2$ catalysts.

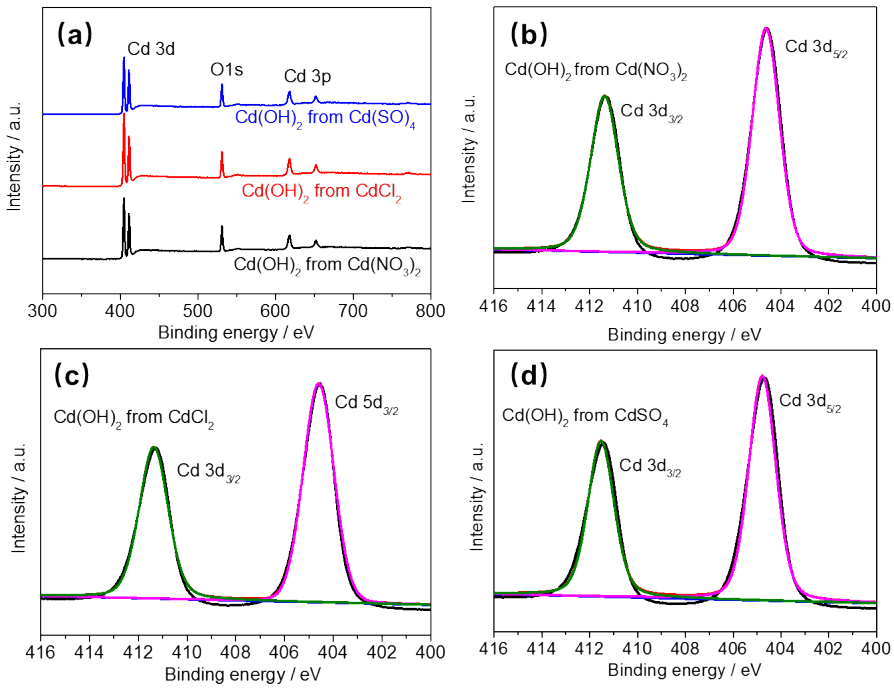

Figure S5. (a) XPS survey spectra and (b,c,d) high-resolution Cd 3d XPS spectra of $Cd(OH)_2$ prepared from $Cd(NO_3)_2$, $CdCl_2$ and $CdSO_4$, respectively.

S7. The OER electrocatalytic activities of $Cd(OH)_2$ prepared by using $CdCl_2$ and $CdSO_4$ as the precursors.

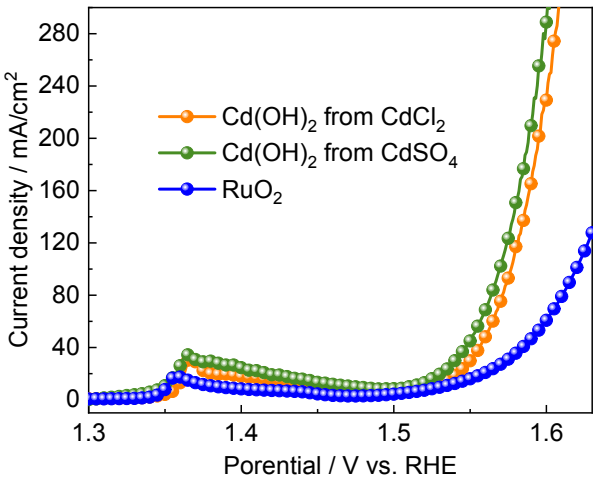

Figure S6. LSV curves of $Cd(OH)_2$ prepared by using $CdCl_2$ and $CdSO_4$ as the precursors.

S8. N_2 adsorption–desorption isotherms of the $Cd(OH)_2$ catalysts.

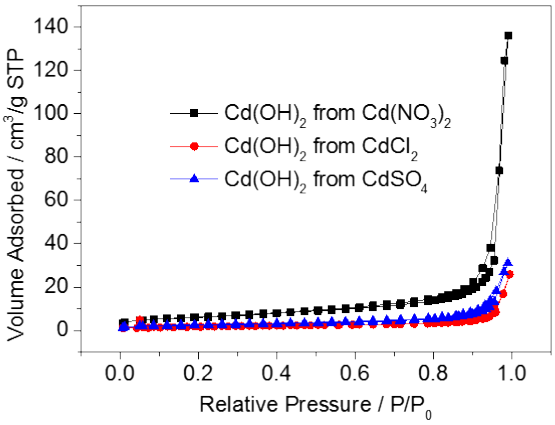

Figure S7. N_2 adsorption–desorption isotherms of the $Cd(OH)_2$ catalysts prepared by using $Cd(NO_3)_2$, $CdCl_2$ and $CdSO_4$ as the precursors.

S9. XRD pattern of $Cd(OH)_2$ catalyst after galvanostatic stability test.

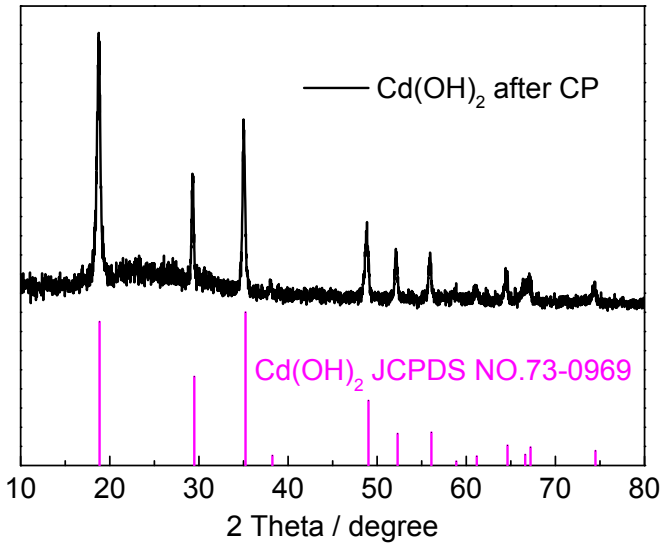

Figure S8. XRD pattern of $Cd(OH)_2$ after chronopotentiometric (CP) experiment.

S10. SEM and TEM images of $Cd(OH)_2$ catalyst after galvanostatic stability test.

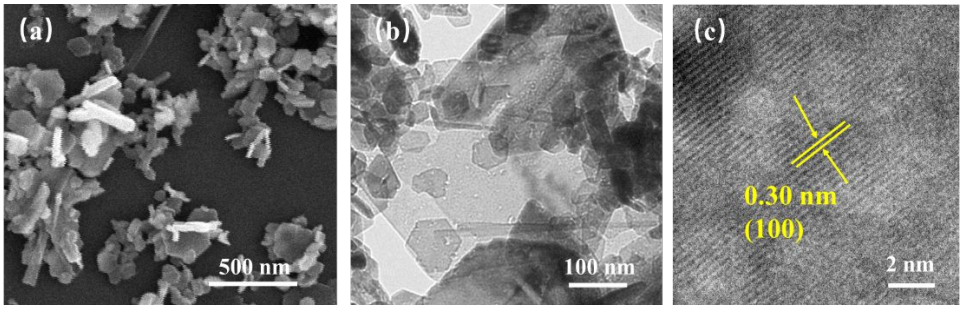

Figure S9. (a) SEM image, (b) TEM image and (c) HRTEM image of $Cd(OH)_2$ catalyst after galvanostatic stability test.

S11. SEM image of $Co(OH)_2$.

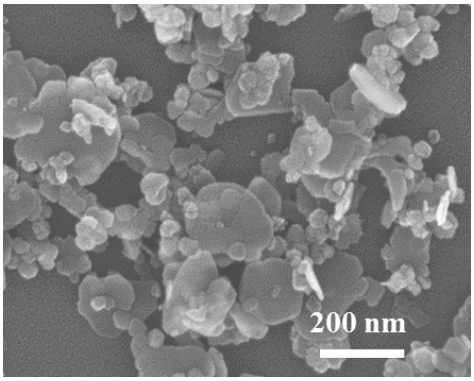

Figure S10. SEM image of $Co(OH)_2$ prepared by using the same method as Cd $(OH)_2$.

S12. The OER electrocatalytic activities of $Fe(OH)_3$ and $Ni(OH)_2$.

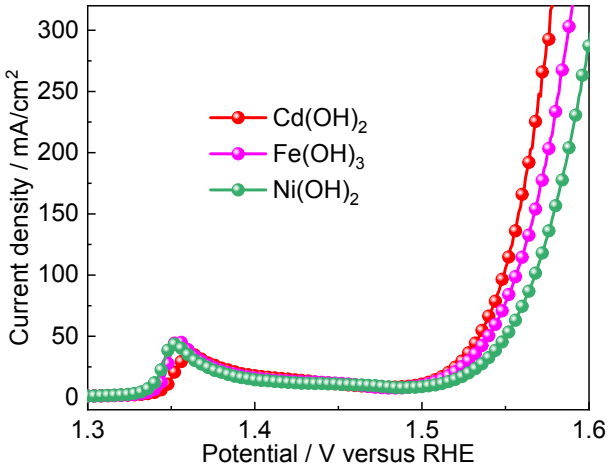

Figure S11. LSV curves of $Cd(OH)_2$, $Fe(OH)_3$ and $Ni(OH)_2$ prepared by the same method.

S13. CV curves of $Cd(OH)_2$ and $Co(OH)_2$ at different scan rates.

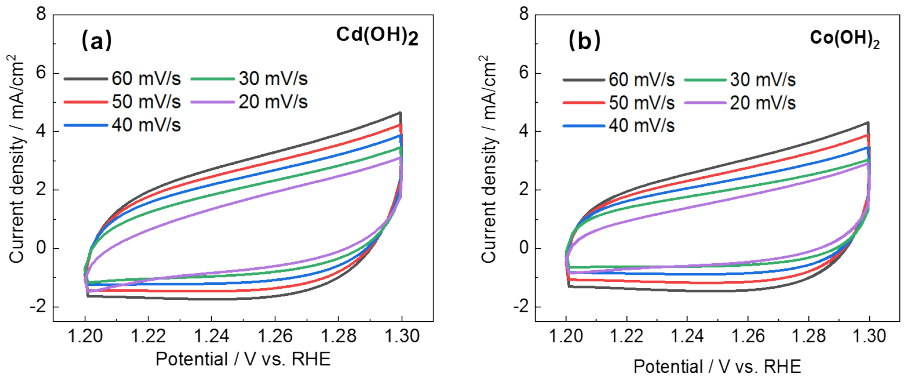

Figure S12. CV curves of (a) Cd $(OH)_2$ and (b) $Co(OH)_2$ in 1.0 M KOH solution at different scan rates.

Supplementary references

S1. Kresse, G., *VASP*. 2014: http://cms.mpi.univie.ac.at/vasp/vasp/vasp.html.

S2. Kresse, G. and J. Furthmuller, *Efficient iterative schemes for ab initio total-energy calculations using a plane-wave basis set.* Phys. Rev. B: Condens. Matter, 1996. **54**(16): p. 11169-11186.

S3. Kresse, G. and D. Joubert, *From ultrasoft pseudopotentials to the projector augmented-wave method.* Phys. Rev. B: Condens. Matter, 1999. **59**(3): p. 1758-1775.

S4. Blochl, P.E., *Projector augmented-wave method.* Phys. Rev. B: Condens. Matter, 1994. **50**(24): p. 17953-17979.

S5. Perdew, J.P., K. Burke, and M. Ernzerhof, *Generalized gradient approximation made simple.* Phys. Rev. Lett. , 1996. **77**(18): p. 3865-3868.

S6. Valdes, A., et al., *Oxidation and photo-oxidation of water on TiO2 surface.* Journal of Physical Chemistry C, 2008. **112**(26): p. 9872-9879.

S7. Rossmeisl, J., et al., *Electrolysis of water on oxide surfaces.* Journal of Electroanalytical Chemistry, 2007. **607**(1-2): p. 83-89.